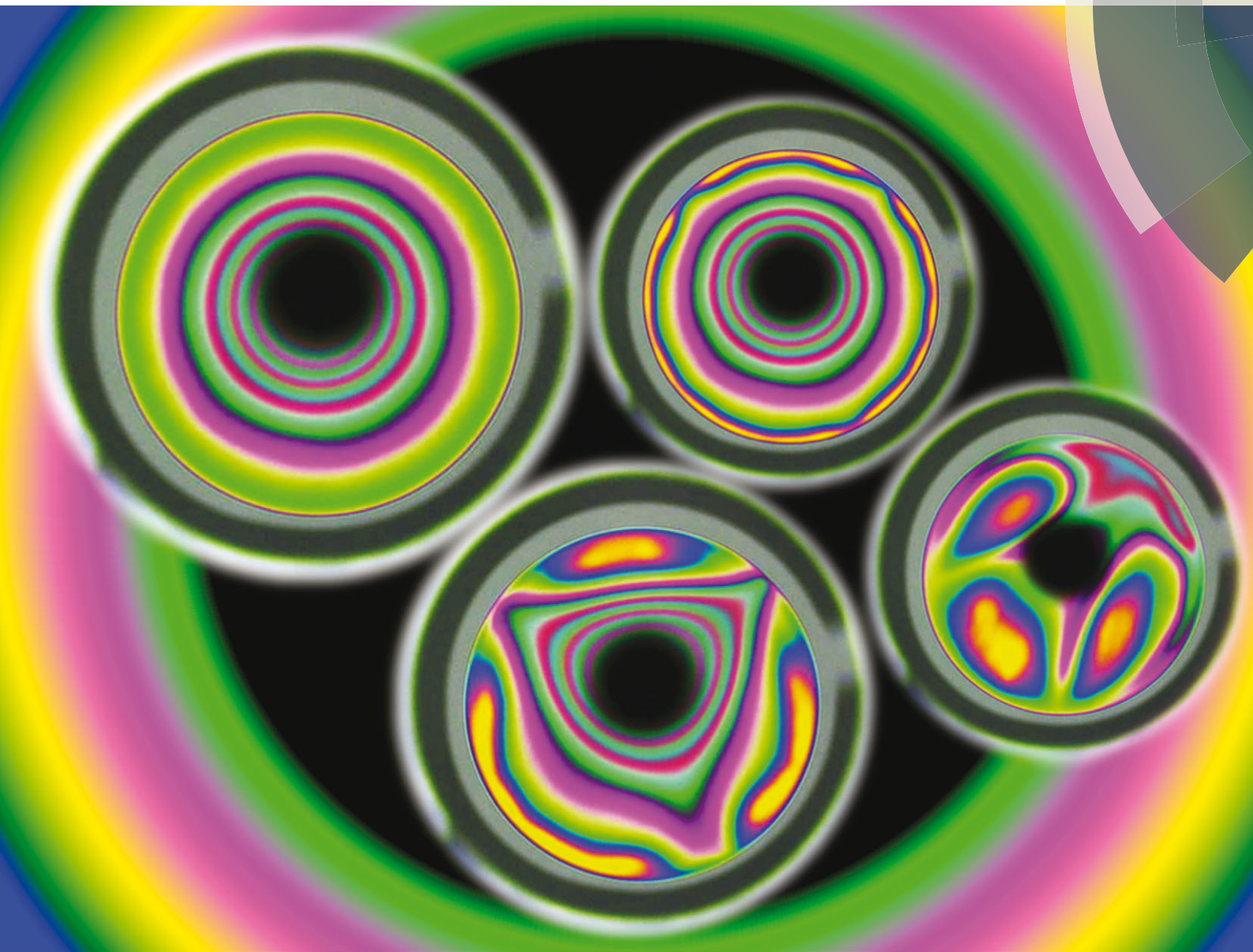


# Soft Matter

[www.softmatter.org](http://www.softmatter.org)



ISSN 1744-683X



**PAPER**

Gerald G. Fuller, Jan Vermant *et al.*  
Lung surfactants and different contributions to thin film stability



Cite this: *Soft Matter*, 2015, **11**, 8048

# Lung surfactants and different contributions to thin film stability†

Eline Hermans,<sup>‡a</sup> M. Saad Bhamla,<sup>‡b</sup> Peter Kao,<sup>c</sup> Gerald G. Fuller<sup>\*b</sup> and Jan Vermant<sup>\*d</sup>

The surfactant lining the walls of the alveoli in the lungs increases pulmonary compliance and prevents collapse of the lung at the end of expiration. In premature born infants, surfactant deficiency causes problems, and lung surfactant replacements are instilled to facilitate breathing. These pulmonary surfactants, which form complex structured fluid–fluid interfaces, need to spread with great efficiency and once in the alveolus they have to form a thin stable film. In the present work, we investigate the mechanisms affecting the stability of surfactant-laden thin films during spreading, using drainage flows from a hemispherical dome. Three commercial lung surfactant replacements Surfacta, Curosurf and Infasurf, along with the phospholipid dipalmitoylphosphatidylcholine (DPPC), are used. The surface of the dome can be covered with human alveolar epithelial cells and experiments are conducted at the physiological temperature. Drainage is slowed down due to the presence of all the different lung surfactant replacements and therefore the thin films show enhanced stability. However, a scaling analysis combined with visualization experiments demonstrates that different mechanisms are involved. For Curosurf and Infasurf, Marangoni stresses are essential to impart stability and interfacial shear rheology does not play a role, in agreement with what is observed for simple surfactants. Surfacta, which was historically the first natural surfactant used, is rheologically active. For DPPC the dilatational properties play a role. Understanding these different modes of stabilization for natural surfactants can benefit the design of effective synthetic surfactant replacements for treating infant and adult respiratory disorders.

Received 29th June 2015,  
Accepted 13th August 2015

DOI: 10.1039/c5sm01603g

[www.rsc.org/softmatter](http://www.rsc.org/softmatter)

## 1 Introduction

Lung surfactant synthesised by alveolar type II cells is a complex mixture of proteins and lipids. It is present as a thin film lining the alveolar surface of the lung with an essential function of lowering the surface tension and the energy for breathing. It also prevents alveolar collapse.<sup>1–4</sup> In addition to the thermodynamic properties, the transport properties are of vital importance. The lung surfactant flows up the terminal airways and reduces the formation of liquid plugs that can obstruct terminal airways at end-expiration.<sup>5–7</sup> Further up the bronchial tree, the intermixing of lung surfactant with airway mucus may improve fluidity and clearance of mucus by cilia on the bronchial epithelium. Taken together, flows of lung surfactant up the airway tree support clearance of inhaled particulates

and pathogens from the alveoli and distal airways, contributing to overall respiratory health.<sup>8</sup> In the neonatal respiratory distress syndrome (NRDS), where naturally occurring surfactant is insufficient, artificial surfactant replacements can be introduced by endotracheal intubation. In this case, both the spreading flow of the surfactants during instillation and the consequent formation of thin stable films are of prime importance.

Natural lung surfactant consists of 80 wt% phospholipids, predominantly dipalmitoylphosphatidylcholine (DPPC), 5 to 10% neutral lipids (mainly cholesterol), and 5 to 10% (surfactant associated) proteins.<sup>9,10</sup> The most common clinically used replacements are natural, animal derived surfactants. They are either extracted from minced cow lung with the addition of DPPC, palmitic acid and tripalmitin (Beractant, trade name Surfacta), extracted from calf lung lavage fluid (Calfactant, trade name Infasurf) or from material obtained from minced pig lung (Poractant, trade name Curosurf). Synthetic surfactants are often based on DPPC.

The complexity of composition is required for different reasons. For example, clinical lung surfactants need to adsorb faster than pure phospholipids. Still, to reach an equilibrium surface tension under physiological conditions, a time scale of minutes is typically required.<sup>11</sup> Past work has focussed on

<sup>a</sup> Department of Chemical Engineering, KU Leuven, Belgium

<sup>b</sup> Department of Chemical Engineering, Stanford University, USA.  
E-mail: [gjf@stanford.edu](mailto:gjf@stanford.edu)

<sup>c</sup> Department of Pulmonary and Critical Care Medicine, Stanford University, USA

<sup>d</sup> Department of Materials, ETH Zürich, Vladimir Prelog Weg 5, CH 8093-Zürich, Switzerland. E-mail: [jan.vermant@mat.ethz.ch](mailto:jan.vermant@mat.ethz.ch)

† Electronic supplementary information (ESI) available. See DOI: 10.1039/c5sm01603g

‡ These authors contributed equally to this work.



understanding of the low level of surface tension in relation to composition. Lung surfactants (and the clinical replacements) adsorb till the surface tension of the air–water interface decreases from 72 to about  $\sim 30 \text{ mN m}^{-1}$ ,<sup>12</sup> or in terms of the surface pressure it increases to  $40 \text{ mN m}^{-1}$ . Though the different clinical surfactants have similar isotherms, AFM studies of deposited layers show fairly different topological features, including multilayer structures or “reservoirs” of fluid phase that are formed beneath the surface.<sup>13–15</sup> These structures are most pronounced in Survanta, and less so in Curosurf or Infasurf.<sup>15</sup> The collapse and respreading of monolayers into multilayers or aggregates have been hypothesised as being essential in the development of the characteristic surface tension area loops associated with pulmonary surfactant at high concentrations.<sup>16,17</sup>

In consideration of the stability of the thin surfactant films, several fluid mechanical processes are apparent. For example the proper functioning of the clinical lung surfactant replacements demands an efficient spreading, followed by the formation of stable thin films that resist rapid thinning and de-wetting. The role of the interfacial viscosity,<sup>13</sup> or more generally interfacial rheology, has been suggested to be of great importance, in addition to the adsorption/desorption dynamics. However, the data on the rheological properties of lung surfactant systems have been reported to vary greatly.<sup>18</sup> Two approaches have been used to investigate the dynamical response of these substances. One approach is to study specific combinations of known elements of the lung surfactant. Hermans and Vermant studied the interfacial shear rheology of DPPC under physiologically relevant conditions.<sup>19</sup> Alonso *et al.* combined DPPC with surfactant protein C (SP-C), and found that this combination led to a highly viscoelastic interface.<sup>20</sup> Zasadzinsky and coworkers systematically added cholesterol to DPPC and found that it dramatically reduced the interfacial shear viscosity.<sup>21–23</sup> In the second approach, which is followed here, clinically approved natural lung surfactant replacements are utilized to mimic *in vitro* lung surfactant as closely as possible. One of the clinical surfactants, Survanta<sup>®</sup>, has been shown to possess a very high surface viscosity.<sup>20</sup> However, it has been reported that other commercially available products differ strongly in their interfacial rheologies.<sup>18</sup>

This paper examines the role of lung surfactants during drainage flows from a hemispherical dome that is quickly raised through the interface and assesses their ability in maintaining stable thin liquid films, under conditions related to fast interfacial deformations. The present work is distinguished from earlier work in two ways. First, there is a comparative rheological characterisation of three clinically most used natural surfactants (Survanta<sup>®</sup>, Curosurf<sup>®</sup>, and Infasurf<sup>®</sup>) as well as DPPC monolayers. Second, we perform a drainage analysis of the same substances, under conditions where adsorption dynamics are not playing a role. A scaling analysis is performed to investigate and separate the mechanisms affecting the stability of surfactant-laden thin films during spreading. Further refinements to replicate the alveolar environment include the lining of the dome surface with alveolar epithelial cells.

## 2 Theoretical background

### 2.1 Different possible contributions to the surface stress

When the interface is deformed, different stresses can arise at the interface, as schematically depicted in Fig. 1. The surface stress is defined as

$$\boldsymbol{\sigma} = \sigma_{\alpha\beta}(\Gamma)\mathbf{I} + \boldsymbol{\sigma}_e \quad (1)$$

where  $\boldsymbol{\sigma}$  is the surface stress tensor,  $\sigma_{\alpha\beta}(\Gamma)$  is the scalar surface tension between two phases  $\alpha$  and  $\beta$  (with  $\alpha$  being the fluid phase and  $\beta$  the air phase),  $\mathbf{I}$  is a  $2 \times 2$  identity tensor,  $\Gamma$  is the surface concentration and  $\boldsymbol{\sigma}_e$  is the deviatoric surface stress tensor. Capillarity will create gradients in bulk pressure when differences in curvature occur. The surface tension will depend on the concentration of the surface active species, and hence the surface tension may vary in time due to adsorption–desorption kinetics when the area of an interface is suddenly changed. However, it should be remarked that an isotropic change in surface tension shall not lead to lateral stresses. Rather, spatial variations (in  $x, y, z$ ) in surface tension are required for this, as they will induce Marangoni stresses. Finally, the response of interfacial microstructures to deformation may give rise to the occurrence of deviatoric stresses of intrinsic rheological origin. We will demonstrate that for the experimental conditions here, neither capillarity nor the adsorption dynamics will play a role. We expect either the rheological response of the interface or Marangoni stresses (or both) to affect the flow and stability of the thin films.

### 2.2 Drainage flow

In Fig. 2, a schematic representation of the experimental geometry is shown. As the film thickness  $h(\theta, t)$  is much smaller than the radius of the dome ( $R$ ), variations of film thickness across the hemisphere are being neglected. We will also show that for the experimental conditions used here, the dome is elevated sufficiently high for capillary effects to be neglected. The flow hence occurs due to drainage from the hemisphere under the action of gravity. As a result, the mathematical problem can be analysed using the lubrication approximation, which reduces the problem to a flat, two-dimensional geometry with a cartesian coordinate system ( $y, \theta$ ). The dominant driving

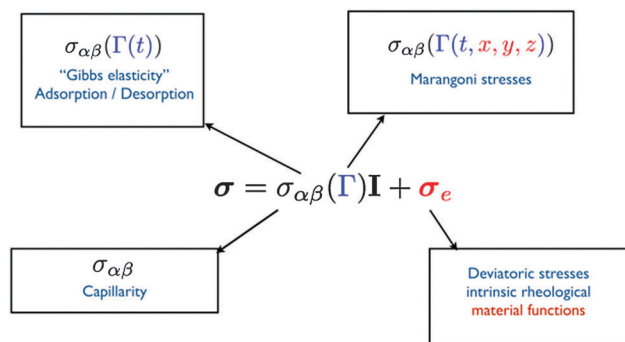
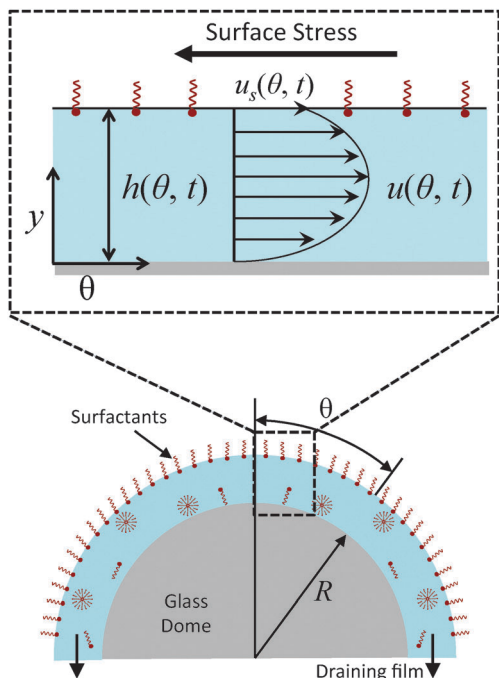


Fig. 1 Potential contributions to the surface stress tensor  $\boldsymbol{\sigma}$  when an interface is deformed and dilated.





**Fig. 2** Schematic illustrating the geometry of the drainage experiment. After being created by raising a dome quickly, a thin film of thickness  $h(\theta, t)$  is drained off a hemispherical dome of radius  $R$ . The inset shows the details of the flow near the apex of the dome on the right side, which include surface stresses arising from surface tension gradients or the rheological characteristics of the interface, counteracting the general driving force for flow, gravity.

force for flow is due to hydrostatic pressure,  $P_h = \rho g h_e$ , where  $h_e$  is the height at which the apex of the dome has been elevated (see Fig. 3, *vide infra*). This pressure must exceed the capillary pressure,  $P_c = 2\sigma_{\alpha\beta}/R$ . The ratio of these two pressures is the Bond number,  $Bo = P_h/P_c = R h_e / 2\lambda^2$ , where  $\lambda = \sqrt{\sigma_{\alpha\beta}/(\rho g)}$  is the capillary length. As demonstrated below our experiments are operated under conditions where  $Bo \gg 1$ .

The evolution of the film thickness in time is fully determined by the velocity profile in the film. In the lubrication limit, the Navier–Stokes equation reduces to eqn (2):

$$\frac{\partial^2 u}{\partial y^2} = -\frac{\rho g}{\eta} \sin \theta \quad (2)$$

This differential equation is completely characterised by the following 2 boundary conditions:  $u|_{y=0} = 0$  (no-slip) and  $u|_{y=h} = u_s(\theta, t)$ . The latter boundary condition recognises that the presence of interfacial agents and their interfacial rheology and/or surface concentration gradients produce a jump in momentum across the interface, due to the occurrence of surface stresses. Solving eqn (2) with respect to the above boundary conditions leads to the following equation for the draining velocity in the film:

$$u = \frac{\rho g}{2\eta} \sin \theta (yh - y^2) + u_s \frac{y}{h} \quad (3)$$

where  $\eta$  is the bulk viscosity of the liquid. It is difficult to directly measure  $u_s$ , the velocity at the interface, with sufficient

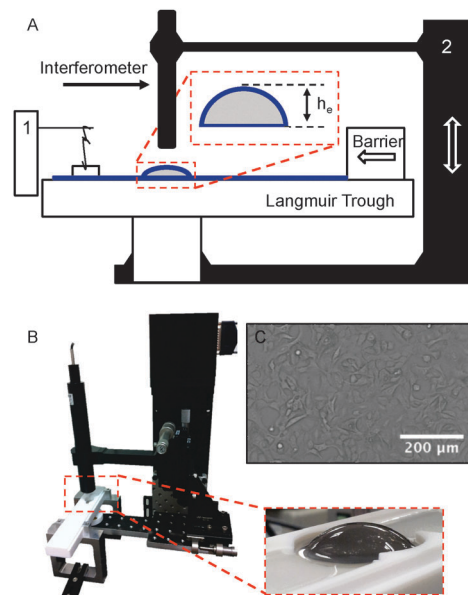


**Fig. 3** Schematic (A) and photograph (B) of the adapted interfacial de-wetting and drainage optical platform (i-DDrOP) with a glass dome on which (C) human alveolar epithelial cells (A549) can be grown to fully mimic *in vivo* conditions. The surface pressure can be controlled using a Langmuir trough (white, Teflon container) and monitored *via* a Wilhelmy balance (1). The dome is elevated through the air–liquid interface using a computer controlled motorised stage (2), and the dome is raised to a height  $h_e$  relative to the planar interface. A high-speed interferometer captures the thickness of this draining film as a function of time, at the apex of the lens ( $\theta = 0$ ).

precision. An easier observable quantity is the thickness of the film as a function of time. Applying conservation of mass leads to the following expression for the evolution of the dimensionless film height,  $H$ , as a function of dimensionless time,  $\tau$ ,

$$\frac{\partial H}{\partial \tau} + \frac{1}{\sin \theta} \frac{\partial}{\partial \theta} \left( \frac{H \sin \theta U_s}{2} + \frac{H^3 \sin^2 \theta}{12} \right) = 0 \quad (4)$$

where  $H = h/h_0$ ,  $\tau = t/T$ ,  $T = \eta R / \rho g h_0^2$  and  $U_s = u_s/(R/T)$ .

### 2.3 Detailed interfacial stress balance

The interfacial stress balance determines the value of  $U_s$  and consists of contributions originating from the surfactant's interfacial rheological characteristics (in both shear and dilation) and Marangoni stresses due to surface tension gradients. Assuming that the interface is Newtonian and neglecting interfacial viscoelasticity, we adopt the commonly used Boussinesq–Scriven model for the interface.<sup>24</sup> Thus, characterising the following parameters for the interface, surface dilatational viscosity,  $\kappa_s$ , and surface shear viscosity,  $\eta_s$ , we can write the tangential interfacial stress balance as

$$\eta_s \frac{\partial u}{\partial y} \Big|_{y=h} = \frac{1}{R} \frac{\partial \sigma_{\alpha\beta}}{\partial \theta} + \frac{\kappa_s}{RT} \dot{\alpha}_s + \eta_s \left( \frac{\dot{\alpha}_s}{RT} + \frac{2u_s}{R^2} \right) \quad (5)$$

where  $\dot{\alpha}_s = \frac{\partial}{\partial \theta} \frac{1}{\sin \theta} \frac{\partial (U_s \sin \theta)}{\partial \theta}$  is related to the rate of change of interfacial area.



The first term on the right, the surface tension gradient  $\frac{\partial \sigma_{\alpha\beta}}{\partial \theta}$ , can be rewritten as  $\frac{\partial \sigma_{\alpha\beta}}{\partial \theta} = \frac{\partial \sigma_{\alpha\beta}}{\partial \Gamma} \cdot \frac{\partial \Gamma}{\partial \theta}$ . The first term measures the rate of change of surface tension with surface concentration,  $\Gamma$ , and the second term corresponds to the gradient of the surfactant concentration across the surface in the  $\theta$ -direction. For the observed velocities ( $> 0.3 \text{ mm s}^{-1}$ ), and as the phospholipids are larger sized molecules than surfactants for which  $D_s$  is well known,<sup>25</sup> the surface Peclet number,  $Pe_s = h_0 u_s / D_s$ , can be estimated to be  $\gg 1$ , and the surfactant transport will be convection dominated. Thus, we can re-write eqn (5) as the tangential stress balance in dimensionless terms as

$$\left. \frac{\partial U}{\partial H} \right|_{H=1} = Bq \Psi^2 \left[ 1 + \Theta \left( 1 + Ma \frac{\partial \Gamma^*}{\partial \theta} \right) \right] \dot{\alpha}_s + 2Bq \Psi^2 U_s \quad (6)$$

where

$$Ma = \frac{\partial \sigma_{\alpha\beta}}{\partial \Gamma^*} \frac{\Gamma^*}{\kappa_s \dot{\alpha}_s / T}, \quad Bq = \frac{\eta_s}{\eta h_0}, \quad \Theta = \frac{\kappa_s}{\eta_s}, \quad \Psi = \frac{h_0}{R}, \quad \Gamma^* = \frac{\Gamma}{\Gamma_{eq}} \quad (7)$$

$Ma$  is the Marangoni number,  $Bq$  is the Boussinesq number and  $\Gamma_{eq}$  is the equilibrium surface concentration. For simplicity we will define  $A$  as

$$A = \left[ 1 + \Theta \left( 1 + Ma \frac{\partial \Gamma^*}{\partial \theta} \right) \right] \quad (8)$$

Analytical solutions to eqn (4) and (6) have been previously obtained in two limits for the time dependence of the film thickness at the apex of the dome ( $\theta = 0$ ) by Bhamla *et al.*<sup>26</sup> The first of these limits is the case of a surfactant free draining liquid layer, where  $Bq = 0$ , while the second limit corresponds to an extremely viscous interface, where  $Bq \rightarrow \infty$ . In both cases, the form of the solution is

$$H = \frac{1}{\sqrt{1 + 4\alpha\tau}} \quad (9)$$

where  $\alpha = 1/3$  for  $Bq = 0$  and  $\alpha = 1/12$  for  $Bq \rightarrow \infty$ . The parameter  $\alpha$  hence enables us to distinguish between a perfectly mobile interface ( $\alpha = 1/3$ ) and an immobile one ( $\alpha = 1/12$ ), where the immobilisation can arise due to rheological properties, providing significant resistance to either shear or dilation, or due to the occurrence of Marangoni stresses. In reporting the experimental data, they will be fit to eqn (9), with  $\alpha$  as a fitting parameter, which will be used as a measure for interfacial immobilisation.

## 3 Materials and methods

### 3.1 Lung surfactant replacements

Three commercial lung surfactant replacements are compared: Curosurf (Chiesi, Italy), Survanta (AbbVie, USA) and Infasurf (ONY Inc., USA). These are, respectively, porcine, bovine and bovine calf surfactants containing 76, 28 and 35 mg phospholipids (PL) per ml (see ESI,† Table S1). Survanta is obtained from minced bovine lung tissue, extracted and precipitated and supplemented with synthetic DPPC, palmitic acid and tripalmitin.<sup>27</sup>

Curosurf comes from minced porcine lung tissue. It is depleted of cholesterol during manufacture.<sup>28</sup> Infasurf is prepared from lung lavage of newborn calves and contains all of the hydrophobic components, including cholesterol.<sup>18</sup> All three were diluted in a phosphate buffered saline (PBS) solution (pH 7.4; Gibco) to identical concentrations of  $0.8 \text{ mg PL ml}^{-1}$ . The concentration was chosen based on the dependence of surface tension on concentration as shown in the ESI,† Fig. S1, where the surface tension of the lung surfactant mixture as measured with a Wilhelmy plate is approximately constant from a concentration of  $0.4 \text{ mg PL ml}^{-1}$  onwards. The clinical lung surfactant replacements were allowed to come to adsorption equilibrium at a temperature of  $37^\circ\text{C}$ , so surface tensions were in the range of  $25\text{--}30 \text{ mN m}^{-1}$  before the start of the drainage experiments. Temperature was maintained at  $37^\circ\text{C}$ , except in the visualisation experiments, which had to be performed at room temperature.

DPPC was procured from Avanti Polar Lipids Inc. (Alabaster, AL) in  $25 \text{ mg ml}^{-1}$  glass vials. Stock solutions of  $1 \text{ mg ml}^{-1}$  in chloroform (Sigma-Aldrich, St. Louis, MO) were created and stored in a freezer until required. DPPC was spread at the interface using chloroform as a spreading solvent and was then compressed to a surface pressure of  $20 \text{ mN m}^{-1}$  before starting any experiment. This particular surface pressure was chosen as to give it the same order of magnitude of surface viscosity as Curosurf and Infasurf (see further).

### 3.2 Interfacial rheology

The double wall ring (DWR) geometry accessory combined with a sensitive magnetic bearing stress rheometer (Discovery HR-3, TA Instruments, USA) and magnetic needle interfacial shear rheometer (ISR) was used to characterise the interfacial rheology of the lung surfactant replacements and the DPPC.<sup>29–31</sup> Only Survanta had sufficiently high viscosities and elasticities to be measured with the DWR, and the other systems were outside of the sensitivity limits and necessitated the use of the ISR. In all cases, the results were corrected for subphase drag as described in the literature.<sup>29–32</sup>

The three lung surfactant replacements were used from their stock solutions as described above and dispersed into the rheometer trough. Following natural adsorption of a monolayer from the bulk fluid and attainment of an equilibrium surface pressure of  $47 \text{ mN m}^{-1}$ , the interfacial rheology was measured. Infasurf and Curosurf interfacial rheologies were obtainable only at room temperature whereas Survanta, being much more viscoelastic, could be studied at  $37^\circ\text{C}$ .

DPPC was spread at the air–water interface in a Langmuir trough by touching microdrops of lipid stock solution ( $1 \text{ mg ml}^{-1}$ ) using a clean Hamilton syringe. We used deionized-distilled water as the subphase from a Milli-Q filtering system (EMD Millipore, Billerica, MA) with a resistivity of  $18.2 \text{ M}\Omega \text{ cm}$  and a surface tension of  $72 \text{ mN m}^{-1}$ . The surface pressure was monitored using a platinum Wilhelmy plate connected to a surface pressure sensor (KSV NIMA Ltd., Helsinki, Finland). The volume of DPPC spread was  $35 \mu\text{l}$ , and the spreading pressure was less than  $0.5 \text{ mN m}^{-1}$ . After chloroform was allowed to evaporate for 30 min, the interface was compressed using symmetric Teflon barriers at a speed



of  $10 \text{ mm min}^{-1}$  till a surface pressure of  $20 \text{ mN m}^{-1}$  was achieved, in order to compare with earlier drainage experiments.<sup>26</sup> The rheology measurements were performed at a strain amplitude of 1%, which is in the linear viscoelastic regime for this material.<sup>19</sup>

### 3.3 Drainage apparatus

To characterise the effect of different substances on film mobility, the drainage of thin films is observed using a modification of the device used previously for the study of tear film lipids.<sup>26,33</sup> A picture and schematic of the instrument are shown in Fig. 3. The device consists of a hemi-spherical glass dome (Newport KPX579) with a (curvature) radius of 19.97 mm mounted on a pedestal that is initially submerged below the air–solution interface. In the case of DPPC, the dome is submerged below an air–liquid interface on which DPPC is spread and then compressed to a known surface pressure. For the lung surfactants barrier compression is not required and experiments are commenced once adsorption to the interface has achieved equilibrium. In both cases, after reaching the desired surface pressure, the dome is elevated using a motorised stage through the interface allowing it to capture a thin liquid film. The thickness of this film is monitored with a high speed white light interferometer (F70, Filmetrics, USA) combined with a halogen light (Fiber-Lite PL-800). A temperature control unit was added to the setup to maintain a temperature of  $37^\circ\text{C}$  during the experiments. Electrical heating elements (Omega) are connected to solid aluminum blocks which are pressed into voids at the bottom of the trough. The thin Teflon bottom in contact with the metal blocks together with a thermocouple feedback system allows for an accurate temperature setting ( $\pm 1^\circ\text{C}$ ) inside the trough.

During the experiments the following protocol was followed. The dome is initially submerged in the trough and positioned approximately  $130 \mu\text{m}$  below the fluid surface. Subsequently, the geometry is raised quickly at a speed of  $10 \text{ mm s}^{-1}$  and the evolution of the film thickness in time is captured by the interferometer at 4 points per second. To compare the drainage results for the different systems and test conditions, the first 4 seconds of height *versus* time data were fitted with eqn (9) to obtain a characteristic value of the fitting parameter  $\alpha$  for every dataset. Drainage of the lung surfactant replacements was investigated for three different conditions: on a clean dome at  $23$  and  $37^\circ\text{C}$  to observe the effect of temperature and additionally on a dome covered with cells at  $37^\circ\text{C}$ . The effect of elevation of the dome has been investigated, as will be discussed below. An elevation of the dome by  $2.5 \text{ mm}$  was used in most experiments, and is in the regime where gravitational stress dominates the capillary stress.

### 3.4 Visualisation of Marangoni stress-induced flows

Past work by Joye *et al.*<sup>34</sup> has shown that film drainage and stability are influenced by both Marangoni stress-induced flows and interfacial rheology. In their work a Scheludko cell was used to reveal the presence of interfacial flow phenomena during drainage. In the present work, we examine drainage flows

associated with bubbles approaching an air–solution interface in the presence of the surfactants employed in this study. To visualise the Marangoni flows, the setup was slightly modified. A spherical air bubble ( $1.1 \text{ mm}$ , dia) was now elevated toward the air–fluid interface. The use of an air bubble instead of a glass dome has the advantage of providing a better index of refraction contrast. The air bubble is generated at the tip of a glass capillary (Drummond Micropipette, Fisher Scientific Inc., MA, USA). The bubble is elevated at a speed of  $0.5 \text{ mm s}^{-1}$  by a vertical distance of  $2 \text{ mm}$ . This ensures that only a fraction of the bubble cap interacts with the air–fluid interface. This thin curved film ( $< 1 \mu\text{m}$ ) under white light illumination ( $420\text{--}780 \text{ nm}$ ) results in colour interference patterns that are captured using a colour CCD camera. These experiments were carried out at room temperature.

### 3.5 Culture of A549 lung epithelial cells

To mimic the alveolar surface, adenocarcinomic human alveolar basal epithelial cells (A549) were purchased from ATCC. They were cultured according to the ATCC guidelines in a F-12K (Kaighn's modification) growth medium (Gibco) enriched with 10% fetal bovine serum (BFS, Gibco) and 1% Pen Strep (penicillin, streptomycin; Gibco). Four days before the drainage experiment, cells were transferred from a full Petri dish to the glass dome. Two-thirds of the cells were deposited in a sterile cup ( $50 \text{ ml}$ ) containing the glass lens on an aluminum pedestal and growth medium. A549 cells are adherent and form a monolayer on top of the geometry (Fig. 3C); no pre-coating was applied to the surface. The remaining one-third of the cells were transferred to a Petri dish as a control for contamination and growth rate. Experiments were performed with domes at a surface coverage of  $> 95\%$ . After two days the growth medium was refreshed.

Prior to drainage experiments, the cell covered geometries were rinsed gently but extensively using a PBS buffer to avoid surface active material from the growth medium to affect results. After 30 minutes the buffer was removed from the trough and replaced by the lung surfactant mixture. Experiments were carried out within one hour to limit cell death.

## 4 Experimental results and discussion

### 4.1 Drainage experiments: introductory remarks

During the drainage experiments, the evolution of the film thickness was monitored in time using an interferometer. A typical result of the height as a function of time for Surfactant and Curosurf (at equal bulk lipid concentration  $0.8 \text{ mg PL ml}^{-1}$ ) and after reaching the equilibrium surface pressure of  $47 \text{ mN m}^{-1}$  is given in Fig. 4. The typical time scale of the experiment is only a few seconds. This time scale was observed to be an order of magnitude smaller than the time scale of adsorption/deposition dynamics, which is on a time scale of minutes.<sup>11</sup> This was confirmed by observations using a Langmuir trough for an area change of 10% (not shown here).

As indicated in Fig. 1, capillary forces can play a role in drainage and stability. However, the importance of these forces



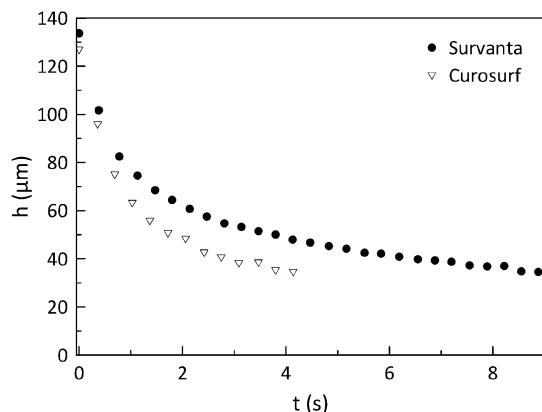


Fig. 4 Typical results of the drainage experiments. The height as a function of time ( $t$ ) for Survanta and Curosurf at 37 °C.

can be diminished by elevating the dome to heights larger than the capillary length of the liquid. The drainage rate was measured for different values of  $h_e$  and, as such, different magnitudes of the hydrostatic pressure. In Fig. 5, the parameter  $\alpha$ , which captures the drainage speed, is plotted *versus*  $Bo = P_H/P_C$ , the ratio of the hydrostatic pressure *versus* capillary pressure. For small  $h_e$  or small  $P_H/P_C$ , the drainage is fast and  $\alpha$  is even larger than the value for the free draining limit of  $1/3$ . After a local minimum, for values of  $P_H/P_C > 10$ , a constant value is obtained for all of the surfactants. This independence also suggests that the initial dilatational deformation that accompanies the deformation of the circle into a hemispherical cap does not have a significant effect on the subsequent drainage and that the initial condition is reproducible.

In the following, we report only experiments at a step height ( $h_e$ ) of 2.5 mm, where  $P_H/P_C > 10$  and from this section it can be concluded that for the experimental conditions used, neither capillarity nor adsorption dynamics will play a major role. For an elevation height of  $h_e = 2.5$  mm and the geometry used, the initial local change in area is 6.8%. We will now investigate if either the rheological response of the interface or

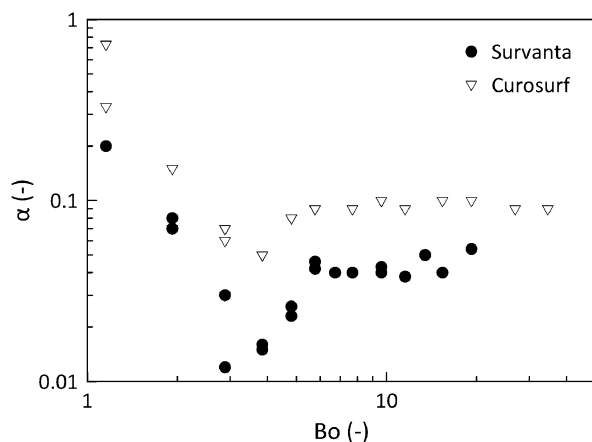


Fig. 5 The drainage rate characterised by the parameter  $\alpha$  for Curosurf and Survanta at room temperature, for different Bond numbers defined as the ratio of hydrostatic pressure ( $P_H$ ) and capillary pressure ( $P_C$ ).

Marangoni stresses, or both, determine the drainage rate and hence govern film stability.

## 4.2 Drainage experiments: experimental results

Fig. 6A showing the results from the interferometry measurements displays how the normalized height ( $H = h/h_0$ ) evolves as a function of dimensionless time ( $\tau$ ), scaled by the gravitational time. The drainage results in Fig. 6A are fit to eqn (9) using only  $\alpha$  as the fitting parameter. A comparison of  $\alpha$  values for all three lung surfactant systems and DPPC is summarized in Fig. 6B. Also shown are  $\alpha$  values for these systems at three different conditions: 25 °C and 37 °C on uncoated surfaces and on a cell-coated surface at 37 °C. The standard deviations for all experiments are calculated from 5 trials or more.

For uncoated surfaces at both temperatures, Infasurf and Curosurf films drain at a similar rate,  $\alpha \sim 0.1$ , which is the value expected for an immobile interface. Survanta films drain significantly slower than the lower limit of the hydrodynamical analysis, by as much as 50% ( $\alpha \sim 0.05$ ). The presence of an

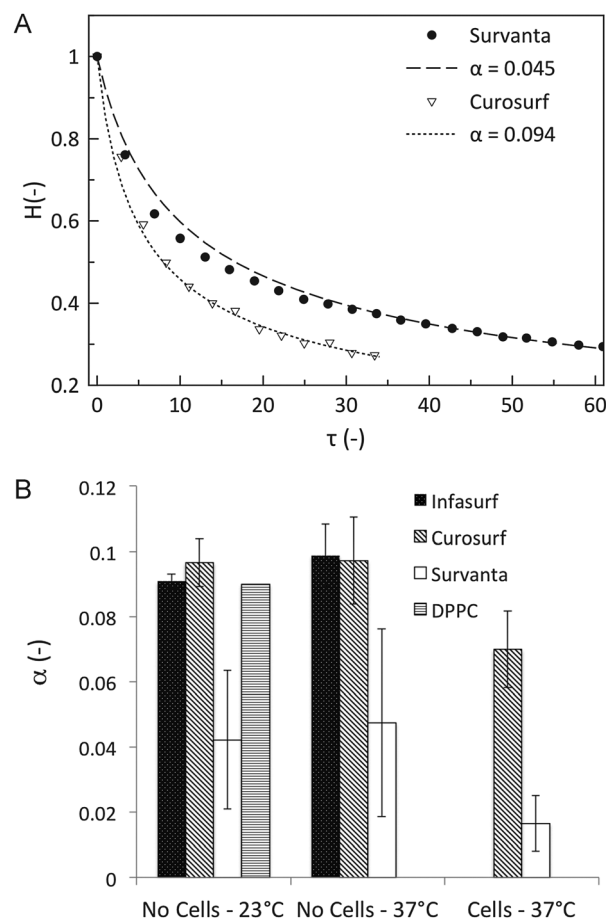


Fig. 6 Results of the drainage experiments. (A) The normalized height ( $H$ ) as a function of rescaled time ( $\tau$ ) for Survanta and Curosurf at 37 °C. The fit of eqn (9) is shown as a dashed line and is used to obtain the fitting parameter  $\alpha$ . (B) The value for the fitting parameter  $\alpha$  for all lung surfactant replacements in the three studied conditions: at 23 °C without cells and at 37 °C with and without cells. The error bars correspond to the stochastic error of minimum 5 experiments.



alveolar epithelial cell monolayer has a striking influence in slowing film drainage. Only results for Curosurf and Survanta are shown here with  $\alpha \sim 0.07$  and  $\alpha \sim 0.02$ , respectively. The different contributions to this reduction in drainage speed will now be investigated and quantified.

### 4.3 Interfacial shear rheology: Bq

To evaluate the effect of the surface rheology, experiments were first performed in shear flow. Linear viscoelastic surface moduli were measured for all four systems and are shown in Fig. 7. Only Survanta films possess strong interfacial viscoelasticity with surface shear moduli,  $G_s'$  and  $G_s'' \sim 10^{-4}$  Pa m. This unusually high viscoelasticity for Survanta is probably due to the presence of palmitic acid and DPPC, as these two components can co-crystallize easily, rendering enhancement of solid phase domains and the possible presence of aggregates protruding in the subphase.<sup>13</sup> Curosurf and Infasurf exhibit interfacial moduli that are two orders of magnitude smaller for both systems and no elastic modulus could reliably be measured. Consequently, the Boussinesq numbers obtained for Curosurf and Infasurf were found to be  $\sim 20$ , making these substances difficult to measure using the ISR.<sup>32</sup> DPPC shows dominantly viscous interfacial shear rheological properties, with the loss modulus  $G_s'' \sim 10^{-5}$  Pa m being slightly larger than that of Curosurf and Infasurf. We desire to map our measured  $\alpha$  values against the Boussinesq numbers that are appropriate for each experiment. From eqn (9), evaluation of this number requires the interfacial viscosity and for this purpose, we use the modulus of the complex viscosity defined as  $|\eta^{s*}| = \frac{\sqrt{G_s'^2 + G_s''^2}}{\omega}$  where the moduli are retrieved from Fig. 7 and  $\omega$  is the lowest accessible frequency.

The theoretical analysis developed in Sections 2.2 and 2.3 can be used to numerically determine the parameter  $\alpha$  as a function of the parameter  $\Delta$  defined in eqn (8). This is shown in

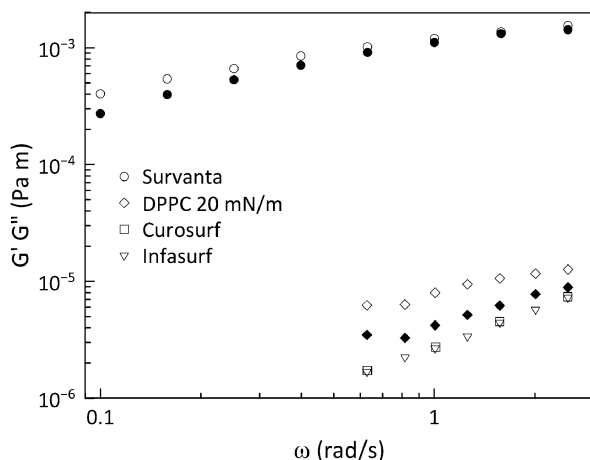


Fig. 7 The linear viscoelastic interfacial moduli as a function of frequency for Survanta, Curosurf and Infasurf at a strain amplitude of 1% and a temperature of 23 °C. The full symbols correspond to  $G'$  and the empty symbols to  $G''$ .

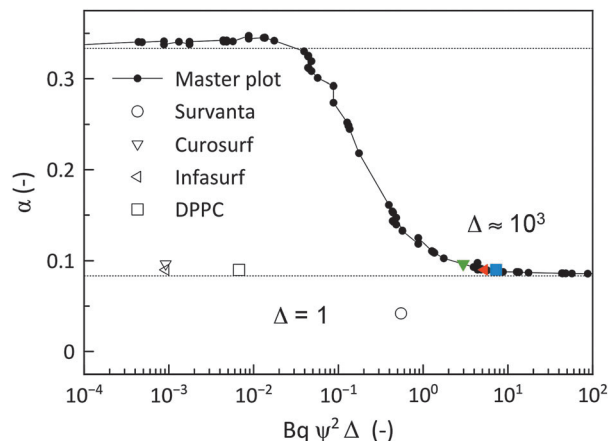


Fig. 8 Mapping of the experimental values of  $\alpha$  for Curosurf (down-pointing open triangle, down-pointing green triangle), Infasurf (left-pointing open triangle, left-pointing red triangle) and DPPC (open square, blue square) onto the numerical solutions of the drainage rate versus  $Bq\psi^2\Delta$  from solving eqn (4) and (6) (black circles). Taking only interfacial shear viscosity ( $\Delta = 1$ , open symbols) does not map the results, and a value of  $\Delta \geq 1000$  is required to map the results (coloured symbols) suggesting important contributions of dilatational viscosity or Marangoni stress.

Fig. 8 along with the data acquired for the lung surfactants and DPPC. There are two sets of experimental data in this plot, one setting  $\Theta$  to zero, and a second set, where the dilatational and Marangoni numbers are adjusted according to a procedure discussed in the following section. The predictions of the model have  $\alpha$  undergo a sharp transition from  $1/3$  (a stress-free interface) to  $1/12$  (a no-slip interface) as  $Bq\psi^2\Delta$  transitions between 0.1 and 1. When only the interfacial shear viscosity of the substances is considered, as was done in previous studies,<sup>19–23,26,33</sup> the theory is unable to capture the experimentally observed response. This discrepancy is resolved by introducing the combined contributions of dilatational rheology and Marangoni stresses.

### 4.4 Dilatational and Marangoni effects: $\Theta$ and $Ma$

It is evident from Fig. 8 that interfacial shear viscosity alone ( $\Delta = 1$ ) cannot describe the measured drainage phenomena. However, by shifting the data laterally, we can estimate the value of the parameter  $\Delta$  that is necessary to bring the theory into alignment with experiments. This translation has been performed in Fig. 8, where it was determined that a value on the order of  $\Delta = 10^3$  is required. Specifically, the  $\Delta$  values for Curosurf, Infasurf, and DPPC are  $3.2 \times 10^3$ ,  $5.7 \times 10^3$ , and  $1.1 \times 10^3$ , respectively. This shifting is not applicable to the drainage data collected for the Survanta system due to its very high interfacial viscoelasticity, as discussed in the following section. It is evident, however, that the other three surfactants stabilise thin films and reduce drainage rates through a combination of dilatational rheology and Marangoni stresses.

The relative importance of interfacial dilatational rheology and Marangoni stresses in drainage dynamics can be assessed directly through visualisation of the thickness variations on thin, draining films. For this purpose, the elevating glass dome



was replaced by an elevating air bubble to enhance the refractive index contrast, creating very strong interference fringes using a colour interferometer. Analogous to the drainage experiments, the bubble is elevated to the air–fluid interface, capturing a thin liquid film that drains back into the surrounding excess reservoir. Under illumination with a white LED light source, these thin films exhibit thin-film color interference, which can be clearly seen in the attached ESI,† videos. A compilation of time-lapse images for all the four surfactant systems is shown in Fig. 9. Using a combination of experiment and theoretical analysis, Joye *et al.*<sup>34</sup> classify the drainage patterns as symmetric and asymmetric. The latter is a typical signature of surface tension driven Marangoni stresses at the interface, caused by dilatation of the air–fluid interface and re-distribution of surfactant molecules at the air–fluid interface. However, Joye *et al.*<sup>34</sup> show that these Marangoni instabilities can be quenched by the presence of dilatational and surface shear viscosities, and surface elasticity, in which case stable and symmetric drainage patterns are typically observed.

The Curosurf and Infasurf films indeed exhibit asymmetric drainage with moderate and highly chaotic surface motions, respectively. These patterns suggest a dominant role of Marangoni stresses in slowing drainage for these films. The low surface shear viscosities point to a very weak structuring at the interface and what is observed is consistent with low molecular weight surfactants. The experiments for DPPC at 20 mN m<sup>−1</sup> show symmetric patterns without any interfacial turbulence over the time span of 20 s, after which the films burst. This symmetric drainage can be qualitatively understood

as having its origin in the small but finite viscoelasticity of this lipid, in agreement with the observations of Joye *et al.*<sup>34</sup> and the occurrence of significant dilatational stresses which quench potential Marangoni stresses. Also shown in Fig. 9 are the time-lapsed interferometric patterns associated with the drainage of Survanta. As in the case of DPPC, this surfactant arrests Marangoni convection due to its large surface viscoelasticity. The drainage behaviour of Survanta is further discussed in the next section.

#### 4.5 Survanta and surface viscoelasticity

The drainage and film stability dynamics of Survanta were observed to be qualitatively different compared to the other surfactants. The observed drainage rate is slower than the lower theoretical limit of 1/12 predicted for an immobile, no-slip interface. As this lower limit corresponds to the state of a zero surface velocity, a further reduced drainage rate might indicate a negative surface velocity towards the apex of the geometry. Only surface tension gradients (Marangoni stress) in the direction of the apex or a mechanical surface elasticity is capable of producing such a recoil effect. It should be noted that in a previously published study with highly viscoelastic meibomian lipids, values of  $\alpha < 1/12$  were obtained,<sup>26</sup> but as yet it is unclear how the surface elasticity couples to the subphase flows. In the visualisation experiments shown in Fig. 9, the Survanta film was observed to be very inhomogeneous, and remained essentially motionless over the lifetime of the film (18 s). This behaviour is characteristic of surfaces exhibiting surface gelation resulting in interfacial elasticity.<sup>35</sup> Thus, the drainage pattern for Survanta and its highly viscoelastic interface (Fig. 7) are in good agreement, but it is not clear how the drainage velocity falls below the immobile limit. Possibly the presence of multilayers in the subphase should also be considered, which could indeed lower the velocity. These aggregate structures are most pronounced in adsorbed Survanta, and less so in Curosurf or Infasurf.<sup>13,15</sup>

## 5 Effect of attached cells on drainage rates

The presence of epithelial cells attached to the glass dome had a significant effect on the drainage rate in comparison to similar experiments on a bare, smooth geometry. In contrast to a smooth geometry, the alveolar epithelial cells induce a microscopic roughness, which slows down the drainage of the fluid film. In the literature, many methods are available to describe the flow of a liquid on top of a rough surface, ranging from flow on a porous layer<sup>36,37</sup> to a surface with distinct obstacles,<sup>38</sup> but the analysis goes beyond the scope of the present work. The result of the surface roughness is that the data can no longer be fitted by a single value of  $\alpha$  and only an average value can be obtained. Fig. 10 shows that the drainage rate, expressed by the fitting parameter  $\alpha$ , decreases in time. This effect will be more pronounced for systems with a low interfacial viscosity in comparison to a high interfacial viscosity.

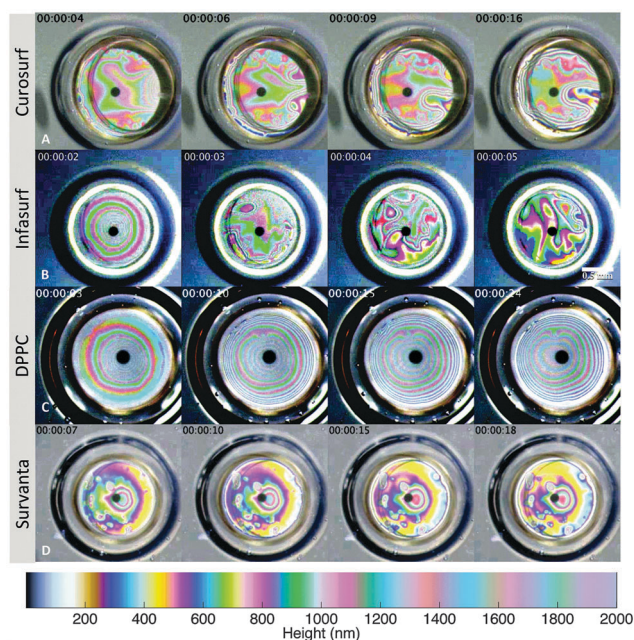


Fig. 9 Snapshots of the interference patterns observed for Curosurf, Infasurf, DPPC and Survanta. The images are captured using the surface flow visualisation setup. The color map is a guide to the eye to relate the vibrant colours to their corresponding thicknesses. The scale bar corresponds to 0.5 mm.



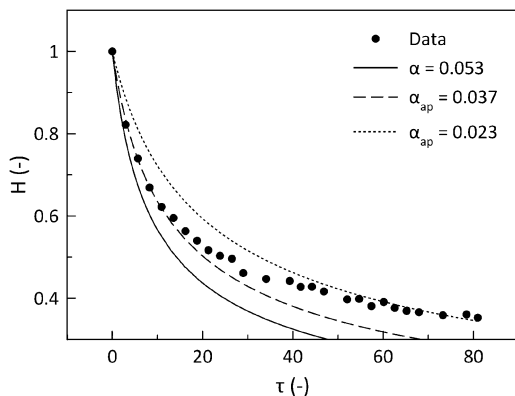


Fig. 10 Experimental results of the normalized height ( $H$ ) as a function of rescaled time ( $\tau$ ) for a Surfactant film flowing over a cell covered geometry at 37 °C. The rate of drainage, expressed by the fitting parameter  $\alpha_{ap}$ , decreases in time due to the portion of flow in the rough layer which becomes more important for thin films.

## 6 Physiological implications

In the present work, both DPPC and clinically approved natural lung surfactant replacements were subjected to a step dilation flow to investigate at least one aspect of thin film stability. The drainage experiments showed that the dominating physical phenomena determining the overall drainage rate differ. For Surfactant and DPPC the interfacial rheological properties play an important, if not dominating, role, whereas for Curosurf and Infasurf they are too weak, resulting in a flow pattern dominated by the local Marangoni gradients.

The studied natural lung surfactant replacements are mainly used for the treatment of the neonatal respiratory distress syndrome (NRDS) in which a liquid bolus is instilled into a baby's lung. The surfactant spreads throughout the lung in a very short time aided by mechanical ventilation and presumably Marangoni flow.<sup>39</sup> This is only possible if the physical properties of the surfactant interface allow fast spreading. Clinical trials comparing the efficiency of the surfactant replacements Curosurf, Infasurf and Surfactant also reveal clinical differences.<sup>40,41</sup> Of course, several factors will contribute to the overall clinical efficacy. What has been shown here is that they all stabilise thin films, but we observe a high surface viscoelasticity for Surfactant. This can be expected to lead to a slower spreading and a different mechanism of stabilising the interface (at least initially). Curosurf and Infasurf are expected to spread better throughout the lung. In the light of designing synthetic lung surfactants, the results of this study suggest that the presence of surface viscoelasticity should be minimised in order to allow Marangoni flows to distribute the lung surfactant more efficiently, while maintaining stability against rapid drainage.

## 7 Conclusion

We have shown that the presence of lung surfactant replacement layers and DPPC monolayers at the air–fluid interface is able to enhance the stability of thin films. Three possible

physical mechanisms were identified: the interfacial shear rheological properties of the interface, the dilatational rheological properties and the presence of Marangoni stresses due to surface tension gradients. Characterisation of the interfacial shear moduli in combination with a mathematical model describing the drainage experiment revealed that the interfacial shear viscosity is not dominant in any of the systems studied. We also showed the relative levels of surface mobility of the surfactants during drainage. These images revealed the importance of Marangoni stresses for the two low viscous surfactants, Curosurf and Infasurf. In the case of DPPC and Surfactant, the local film mobility was much smaller, indicating a relatively strong contribution of the dilatational properties for DPPC and shear surface elasticity in the case of Surfactant. More broadly, a fundamental understanding of the different stabilisation mechanisms of natural lung surfactants may give clues for engineering synthetic replacements for treatment of the respiratory distress syndrome.

## Acknowledgements

The authors would like to thank FWO Vlaanderen for PhD Fellowship to E.H. Chiesi Farmaceutici is gratefully acknowledged for providing Curosurf and AbbVie for providing Surfactant. We would like to thank Benoit Scheid (ULB, Belgium) for fruitful discussions and Y. Strakovsky (Stanford University) for contributions to the design of graphics and schematics. Finally, we would like to thank Joannes Vermant, Chew Chai and Marco A. Álvarez-Valenzuela for their help with the Marangoni bubble experiments, and Javier Tajuelo for discussions on the ISR.

## References

- 1 R. E. Pattle, Properties, function and origin of the alveolar lining layer, *Nature*, 1955, **175**, 1125–1126.
- 2 R. E. Pattle, Surface lining of lung alveoli, *Phys. Rev.*, 1965, **45**, 48–79.
- 3 E. S. Brown, R. P. Johnson and J. A. Clements, Pulmonary surface tension, *J. Appl. Physiol.*, 1958, **14**, 717–720.
- 4 J. A. Clements, R. F. Hustead, R. P. Johnson and I. Gribetz, Pulmonary surface tension and alveolar stability, *J. Appl. Physiol.*, 1961, **16**, 444–450.
- 5 D. Halpern, H. Fujioka, S. Takayama and J. B. Grotberg, Liquid and surfactant delivery into pulmonary airways, *Respir. Physiol. Neurobiol.*, 2008, **163**, 222–231.
- 6 K. Koch, *et al.* Surface tension gradient driven spreading on aqueous mucin solutions: a possible route to enhanced pulmonary drug delivery, *Mol. Pharmaceutics*, 2011, **8**, 387–394.
- 7 R. Levy, D. B. Hill, M. G. Forest and J. B. Grotberg, Pulmonary Fluid Flow Challenges for Experimental and Mathematical Modeling, *Integr. Comp. Biol.*, 2014, **54**, 985–1000.
- 8 A. Podgorski and L. Gradon, Dynamics of pulmonary surfactant system its role in alveolar cleansing, *Ann. Occup. Hyg.*, 1990, **34**, 137–147.



- 9 J. Goerke and J. A. Clements, Pulmonary surfactant: an engineering marvel, In: *Proc. Ann. Int. Conf. – IEEE Eng., Med. Biol.*, 1999, **1**, 355.
- 10 J. Perez-Gil and T. E. Weaver, Pulmonary Surfactant Pathophysiology: Current Models and Open Questions, *Physiology*, 2010, **25**, 132–141.
- 11 R. H. Notter, J. N. Finkelstein and R. D. Taubold, Comparative adsorption of natural lung surfactant, extracted phospholipids, and artificial phospholipids mixtures to the air water interface, *Chem. Phys. Lipids*, 1983, **33**, 67–80.
- 12 S. Schurch, J. Goerke and J. A. Clemnets, Direct determination of volume-dependence and time-dependence of alveolar surface-tension in excised lungs, *Proc. Natl. Acad. Sci. U. S. A.*, 1978, **75**, 3417–3421.
- 13 C. Alonso, T. Alig, J. Yoon, F. Bringezu, H. Warriner and J. Zasadzinski, More than a monolayer: relating lung surfactant structure and mechanics to composition, *Biophys. J.*, 2004, **87**, 4188–4202.
- 14 H. Bachofen, *et al.* Structures of pulmonary surfactant films adsorbed to an air–liquid interface in vitro, *Biochim. Biophys. Acta, Biomembr.*, 2005, **1720**, 59–72.
- 15 H. Zhang, Q. Fan, Y. E. Wang, C. R. Neal and Y. Y. Zuo, Comparative study of clinical pulmonary surfactants using atomic force microscopy, *Biochim. Biophys. Acta, Biomembr.*, 2011, **1808**, 1832–1842.
- 16 S. R. Schürch, H. Qanbar, H. Bachofen and F. Possmayer, The surface associated surfactant reservoir in the alveolar lining, *Biol. Neonate*, 1995, **67**, 61–67.
- 17 A. Von Nahmen, M. Schenk, M. Sieber and M. Amrein, The structure of a model pulmonary surfactant as revealed by scanning force microscopy, *Biophys. J.*, 1997, **72**, 463–469.
- 18 M. Rudiger, A. Tolle, W. Meier and B. Rustow, Naturally derived commercial surfactants differ in composition of surfactant lipids and in surface viscosity, *Am. J. Physiol.*, 2005, **288**, L379–L383.
- 19 E. Hermans and J. Vermant, Interfacial shear rheology of DPPC under physiologically relevant conditions, *Soft Matter*, 2014, **10**, 175–186.
- 20 C. Alonso, A. Waring and J. A. Zasadzinski, Keeping lung surfactant where it belongs: protein regulation of two-dimensional viscosity, *Biophys. J.*, 2005, **89**, 266–273.
- 21 K. Kim, S. Q. Choi, Z. A. Zell, T. M. Squires and J. A. Zasadzinski, Effect of cholesterol nanodomains on monolayer morphology and dynamics, *Proc. Natl. Acad. Sci. U. S. A.*, 2013, **110**, 3054–3060.
- 22 K. Kim, S. Q. Choi, J. A. Zasadzinski and T. M. Squires, Interfacial microrheology of DPPC monolayers at the air–water interface, *Soft Matter*, 2011, **7**, 7782–7789.
- 23 S. Q. Choi, *et al.* Influence of molecular coherence on surface viscosity, *Langmuir*, 2014, **30**, 8829–8838.
- 24 L. E. Scriven, Dynamics of a fluid interface, equation of motion of newtonian surface fluids, *Chem. Eng. Sci.*, 1960, **12**, 98–108.
- 25 D. C. Clark, *et al.* Surface diffusion in sodium dodecyl sulfate-stabilized thin liquid films, *J. Colloid Interface Sci.*, 1990, **138**, 195–206.
- 26 M. S. Bhamla, C. E. Giacomini, C. Balemans and G. G. Fuller, Influence of interfacial rheology on drainage from curved surfaces, *Soft Matter*, 2014, **10**, 6197–6206.
- 27 R. H. Notter, Z. Wang, E. A. Egan and B. A. Holm, Component-specific surface and physiological activity in bovine-derived lung surfactants, *Chem. Phys. Lipids*, 2002, **114**, 21–34.
- 28 O. Blanco and J. Perez-Gil, Biochemical and pharmacological differences between preparations of exogenous natural surfactant used to treat respiratory distress syndrome: role of the different components in an efficient pulmonary surfactant, *Eur. J. Pharmacol.*, 2007, **568**, 1D15.
- 29 S. Vandebril, A. Franck, G. G. Fuller, P. Moldenaers and J. Vermant, A double wall-ring geometry for interfacial shear rheometry, *Rheol. Acta*, 2010, **49**, 131–144.
- 30 C. F. Brooks, G. G. Fuller, C. W. Curtis and C. W. Robertson, An interfacial stress rheometer to study rheological transitions in monolayers at the air–water interface, *Langmuir*, 1999, **15**, 2450–2459.
- 31 S. Reynaert, C. F. Brooks, P. Moldenaers, J. Vermant and G. G. Fuller, Analysis of the magnetic rod interfacial stress rheometer, *J. Rheol.*, 2008, **52**, 261–285.
- 32 T. Verwijlen, P. Moldenaers, H. A. Stone and J. Vermant, Study of the flow field in the magnetic rod interfacial stress rheometer, *Langmuir*, 2011, **27**, 9345–9358.
- 33 M. S. Bhamla, C. Balemans and G. G. Fuller, Dewetting and deposition of thin films with insoluble surfactants from curved silicone hydrogel substrates, *J. Colloid Interface Sci.*, 2015, **449**, 428–435.
- 34 J. L. Joye, G. J. Hirasaki and C. A. Miller, Asymmetric drainage in foam films, *Langmuir*, 1994, **10**, 3174–3179.
- 35 C. Monteux, *et al.* Adsorption of oppositely charged polyelectrolyte/surfactant complexes at the air/water interface: formation of interfacial gels, *Langmuir*, 2004, **20**, 57–63.
- 36 G. S. Beavers and D. D. Joseph, Boundary conditions at a naturally permeable wall, *J. Fluid Mech.*, 1967, **30**, 197–207.
- 37 C. Carotenuto and M. Minale, Shear flow over a porous layer: velocity in the real proximity of the interface via rheological tests, *Phys. Fluids*, 2011, **23**, 063101.
- 38 J. Seiwert, M. Maleki, C. Clanet and D. Quéré, Drainage of a rough surface, *EPL*, 2011, **94**, 16002.
- 39 K. J. Cassidy, *et al.* A rat lung model of instilled liquid transport in the pulmonary airways, *J. Appl. Phys.*, 2001, **90**, 1955–1967.
- 40 C. A. Malloy, P. Nicoski and J. K. Muraskas, A randomized trial comparing beractant and poractant treatment in neonatal respiratory distress syndrome, *Acta Paediatr.*, 2007, **94**, 779–784.
- 41 R. Ramanathan, *et al.* A randomized, multicenter masked comparison trial of Poractant alfa (Curosurf) versus Beractant (Survanta) in the treatment of respiratory distress syndrome in preterm infants, *Am. J. Perinat.*, 2004, **21**, 109–119.

